Marine Chemistry 205 (2018) 16–28

Contents lists available at ScienceDirect

Marine Chemistry

journal homepage: www.elsevier.com/locate/marchem

Seasonal variability of carbonate chemistry and decadal changes in waters of a marine sanctuary in the Northwestern Gulf of Mexico

Xinping Hu[a,*], Marissa F. Nuttall[b,c], Hongjie Wang[a], Hongming Yao[a], Cory J. Staryk[a], Melissa R. McCutcheon[a], Ryan J. Eckert[b,1], John A. Embesi[b,c], Michelle A. Johnston[b], Emma L. Hickerson[b], George P. Schmahl[b], Derek Manzello[d], Ian C. Enochs[d,e], Steven DiMarco[f], Leticia Barbero[d]

[a] Department of Physical and Environmental Sciences, Texas A&M University–Corpus Christi, Corpus Christi, TX 78412, United States
[b] NOAA Office of National Marine Sanctuaries, Flower Garden Banks National Marine Sanctuary, Galveston, TX 77551, United States
[c] CPC, San Diego, CA 92108, United States
[d] Atlantic Oceanographic and Meteorological Laboratory, NOAA, Miami, FL 33149, United States
[e] Cooperative Institute for Marine and Atmospheric Studies, Rosenstiel School of Marine and Atmospheric Science, University of Miami, Miami, FL 33149, United States
[f] Department of Oceanography, Texas A&M University, College Station, TX 77843, United States

ARTICLE INFO

Keywords:
Coral reef
Ocean acidification
Gulf of Mexico
Flower Garden Banks National Marine Sanctuary
Anthropogenic CO_2

ABSTRACT

We report seasonal water column carbonate chemistry data collected over a three-year period (late 2013 to 2016) at Flower Garden Banks National Marine Sanctuary (FGBNMS) located on the subtropical shelf edge of the northwestern Gulf of Mexico. The FGBNMS hosts the northernmost tropical coral species in the contiguous United States, with over 50% living coral cover. Presented here are results from samples of the upper 25 m of the water column collected from September 2013 to November 2016. Additionally, following a localized mortality event likely associated with major continental flooding in summer 2016, water samples from up to ~250 m depth were collected in the broader FGBNMS area on a rapid response cruise to examine the seawater carbonate system. Both surface (< 5 m) total alkalinity (TA) and total dissolved inorganic carbon (DIC) vary over small ranges ($2391 \pm 19\,\mu mol\,kg^{-1}$ and $2060 \pm 19\,\mu mol\,kg^{-1}$, respectively) for all times-series samples. Temperature and salinity both played an important role in controlling the surface water carbonate system dynamics, although temperature was the sole significant factor when there was no flooding. The FGBNMS area acted as a sink for atmospheric CO_2 in winter and a CO_2 source in summer, while the time-integrated CO_2 flux is close to zero (-0.14 ± 1.96 mmol-C $m^{-2}\,yr^{-1}$). Results from three cruises, i.e., the Gulf of Mexico and East Coast Carbon Project (GOMECC-1) in 2007, the rapid response study, and the Gulf of Mexico Ecosystems and Carbon Cruise (GOMECC-3), revealed decreases in both pH and saturation state with respect to aragonite (Ω_{arag}) in subsurface waters (~100–250 m) over time. These decreases are larger than those observed in other tropical and subtropical waters. Based on reaction stoichiometry, calculated anthropogenic CO_2 contributed 30–41% of the overall DIC increase, while elevated respiration accounted for the rest.

1. Introduction

Coral reefs in low latitude environments have attracted considerable attention from the scientific community as these environments provide significant ecosystem services. However, current climatic and ocean chemistry changes threaten important reef organisms and the skeletal structures they provide, including decreasing coral grow rates under warmer conditions (Cantin et al., 2010), decreasing coral calcification rates (Erez et al., 2011; Hoegh-Guldberg et al., 2007; Kleypas and Yates, 2009), decreasing coral skeletal density (Mollica et al., 2018), and even enhanced dissolution of coral sand (Eyre et al., 2018) under current ocean acidification conditions. There are, however, coral reefs and coral communities in higher latitude environments, such as in the northwestern Gulf of Mexico, with distributions constrained by temperature and light availability, which are also ecologically and economically important (DeBose et al., 2013; Kleypas et al., 2001; Johnston et al.,

* Corresponding author.
E-mail address: xinping.hu@tamucc.edu (X. Hu).
[1] Current address: Harbor Branch Oceanographic Institute, Florida Atlantic University, 5600 US 1 North, Fort Pierce, FL 34946.

https://doi.org/10.1016/j.marchem.2018.07.006
Received 6 November 2017; Received in revised form 26 June 2018; Accepted 14 July 2018
Available online 17 July 2018

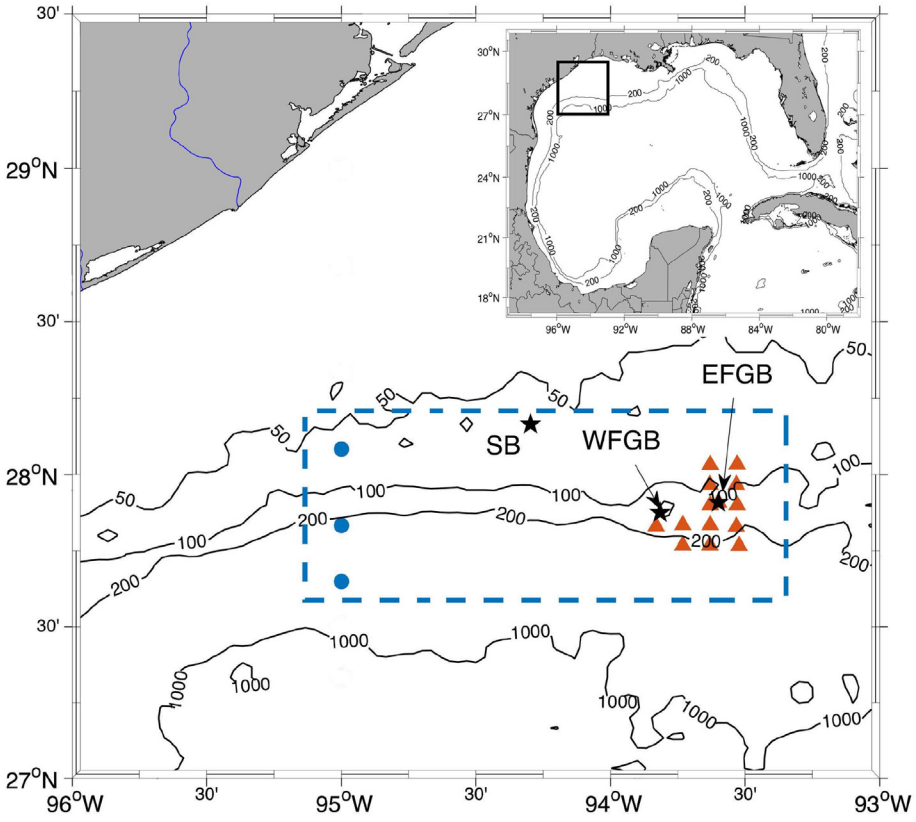

Fig. 1. Sampling stations (filled circles) of the 2007 GOMECC-1 and the 2017 GOMECC-3 cruises both on board *R/V* Ron Brown (Galveston transect) and the 2016 rapid response cruise on board *R/V* Manta (filled triangles). Data from the three stations from the GOMECC cruises within the rectangle were chosen to compare with those from 2016. Stetson Bank (SB), West Flower Garden Bank (WFGB), and East Flower Garden Bank (EFGB) are marked with filled stars. Note that both EFGB and WFGB are sitting on the 100 m isobath. The square in the map insert shows the general sampling area in this study.

2016). Coral communities of the Flower Garden Banks National Marine Sanctuary in the northwestern Gulf of Mexico (FGBNMS, Fig. 1), part of the federally managed National Marine Sanctuary System protecting submerged sites of national significance under *The National Marine Sanctuaries Act*, represent the northernmost tropical species around the contiguous United States (Bright, 1977; DeBose et al., 2013; Johnston et al., 2017a; Lang et al., 2001). FGBNMS consists of three separate banks (Fig. 1) - East Flower Garden Bank (EFGB), West Flower Garden Bank (WFGB), and Stetson Bank (SB) - located along the outer continental shelf (Johnston et al., 2017a). Whereas annual monitoring to document the benthic and fish communities has been conducted at these sites since 1989 (EFGB and WFGB) and 1993 (SB), the biogeochemical characteristics of this area are not fully understood.

Corals in the FGBNMS region, living in marginal environmental conditions for their development and growth (DeBose et al., 2013), are subject to greater temperature fluctuations than their counterparts in the tropical Atlantic, especially for the SB location that is closest to land. Additionally, occasional continental flooding introduces freshwater that depresses seawater salinity and hurricanes cause physical disturbance to the benthic environment in these outer shelf regions (Robbart et al., 2008). Therefore, understanding both spatial and temporal variability of the physicochemical conditions of these coral habitats and their long-term changes is important.

Monitoring of water quality parameters (temperature, salinity, chlorophyll, nitrate, nitrite, phosphorus, and ammonia) at the EFGB and WFGB sites started in 1989 as part of a long-term program (Johnston et al., 2017a), shortly before the establishment of the marine sanctuary in 1992. Seawater carbonate system characterization was not included in this monitoring program until late 2013 with the initiation of biennial sampling as part of NOAA's National Coral Reef Monitoring Program (NCRMP) (NOAA Coral Program, 2014). In November 2013, the Carbon Cycle Laboratory (CCL) at Texas A&M University–Corpus Christi partnered with FGBNMS to start seawater sample collection for carbonate system analysis on a roughly quarterly basis at all three FGBNMS sites, as a complement to the sanctuary's long-term monitoring program (Johnston et al., 2017a; Nuttall et al., 2017).

In this study, we examined seasonal variability of both measured and derived carbonate system parameters (total alkalinity or TA, total dissolved inorganic carbon or DIC, pH, saturation state with respect to aragonite or Ω_{arag}, and partial pressure of CO_2 or pCO_2) in the water column of FGBNMS and identified the controlling factors of these parameters. We also compared decadal changes in water column carbonate system parameters using data from a rapid response cruise following a localized mortality event at the EFGB in the summer of 2016 (Johnston et al., 2017b) and two cross-shelf cruises that sampled an area close to the FGBNMS in the summers of 2007 and 2017, i.e., the first Gulf of Mexico and East Coast Carbon Project (GOMECC-1) and the Gulf of Mexico Ecosystems and Carbon Cruise (GOMECC-3) (Table 1). The three stations chosen from the GOMECC cruises are about 150 km and 80 km to the west of EFGB and SB, respectively (Fig. 1).

2. Materials and methods

2.1. Study sites

Underlying all three FGBNMS banks within the sanctuary boundaries are salt dome formations with salt deposits from the Jurassic, a common occurrence in the northern Gulf of Mexico. EFGB and WFGB, approximately 190 km south of the Texas-Louisiana border, range in depth from 16 to 150 m and are capped with coral reef communities with > 50% living coral cover (Fig. 1). SB, considered a mid-shelf bank, is located approximately 56 km northwest of WFGB and approximately 100 km offshore (Fig. 1). SB is an uplifted claystone feature ranging in depth from 17 to 53 m and capped with coral and sponge communities (Nuttall et al., 2017). All these banks provide three-dimensional hard bottom habitats and support diverse communities of hermatypic corals, black corals, and octocorals, in addition to abundant fish and invertebrate communities. Due to the closer proximity of SB to shore,

Table 1
Sampling dates and analyzed parameters in the FGBNMS and adjacent areas.

Cruise	Sampling dates	Sampling sites[a]	Measured parameters[b]	Variables for speciation calculations
GOMECC-1	07/11/2007	West of FGBNMS, Fig. 1	DIC, TA, nutrients, DO	DIC, TA, nutrients
NCRMP	09/02–09/06, 2013	E, W	DIC, TA	DIC, TA
FGBNMS-WQ	11/18, 2013	E, W, S	DIC, TA, pH (unpurified mCP)	DIC, TA
FGBNMS-WQ	05/16–05/17, 2014	E, W, S	DIC, TA, pH (purified mCP)	DIC, pH
FGBNMS-WQ	09/09–09/10, 2014	E, W, S	DIC, TA, pH (purified mCP)	DIC, pH
FGBNMS-WQ	11/10, 2014	E, W, S	DIC, TA, pH (purified mCP)	DIC, pH
FGBNMS-WQ	02/10–02/11, 2015	E, W, S	DIC, TA, pH (purified mCP)	DIC, pH
FGBNMS-WQ	05/01/2015	E, W, S	DIC, TA, pH (purified mCP)	DIC, pH
NCRMP	08/24–08/28, 2015	E, W	DIC, TA	DIC, TA
FGBNMS-WQ	10/08/2015	S	DIC, TA, pH (purified mCP)	DIC, pH
FGBNMS-WQ	11/04/2015	E, W, S	DIC, TA, pH (purified mCP)	DIC, pH
FGBNMS-WQ	02/18/2016	E, W, S	DIC, TA, pH (purified mCP)	DIC, pH
FGBNMS-WQ	05/19/2016	E, W, S	DIC, TA, pH (purified mCP)	DIC, pH
Rapid response	08/01/2016	Multiple stations, Fig. 1	DIC, TA, pH (purified mCP), DO	DIC, pH
FGBNMS-WQ	08/12/2016	E, W, S	DIC, TA, pH (purified mCP)	DIC, pH
FGBNMS-WQ	11/15/2016	E, W, S	DIC, TA, pH (purified mCP)	DIC, pH
GOMECC-3	07/31/2017	West of FGBNMS, Fig. 1	DIC, TA, nutrients, DO	DIC, TA, nutrients

[a] E, W, and S represent EFGB, WEGB, and SB, respectively.
[b] Samples from the NCRMP cruises, all Flower Garden Bank National Marine Sanctuary Water Quality (FGBNMS-WQ) cruises, and the rapid response cruise all analyzed using an open-cell Gran titration technique for TA analysis and infrared detection for DIC analysis (Hu et al., 2017). TA from GOMECC-1 and GOMECC-3 cruises as measured using open-cell and close-cell Gran titration, respectively, although DIC was measured coulometrically (Dickson et al., 2007). All spectrophotometric pH measurements were done at 25 °C except for the November 2013 cruise, when we used unpurified mCP at 21 °C. All dissolved oxygen concentrations (DO) were measured using Winkler titration. All cruises had in-situ temperature, pressure, and salinity data collected by CTD.

more variable temperature regimes and water clarity have been observed at SB than at EFGB and WFGB (Nuttall et al., 2017).

2.2. Sample collection and analytical methods

Two cruises (September 2013 and August 2015) were conducted to collect discrete water samples at the FGBNMS as part of NOAA's NCRMP (Table 1). Surface water samples were collected in 500 ml borosilicate glass bottles ($n = 22$ in 2013 and $n = 23$ in 2015) and immediately preserved with 200 µl of a saturated $HgCl_2$ solution. These samples were analyzed at NOAA's Atlantic Oceanographic and Meteorological Laboratory (AOML) (Table 1).

Starting in November 2013, in partnership with the FGBNMS, water samples were collected on board the R/V *Manta* from three depths (surface, mid depth, and bottom) at all three FGBNMS sites on a quarterly basis (Table 1). In response to a localized mortality event observed at the end of July 2016 (Johnston et al., 2017b), 14 stations that covered both EFGB and WFGB sites and ranged from the reef crest to water depths at up to 250 m were also sampled on board the R/V *Manta* on August 1, 2016 (Fig. 1, Table 1). All sample collections followed the standard sampling protocols described in Dickson et al. (2007). Briefly, water samples were transferred from the Niskin bottles into 250-ml ground-neck borosilicate glass bottles, to which 100 µl of a saturated $HgCl_2$ solution were added before the bottles were sealed using glass stoppers with the aid of Apiezon® L grease and rubber bands. All samples for shore-based analyses were kept refrigerated at 4 °C in the dark, with the exceptions of two occasions (November 2013 and November 2014), when the samples were stored in 60 ml plastic syringes with stopcocks in a water bath (21 °C in 2013 and 25 °C in 2014) for less than one hour before pH analysis on board the ship. Nutrient samples were also collected from surface water (bucket) and near bottom (within 0.5 m of the bottom using Niskin bottles) and frozen until analysis.

Two cruises on the R/V *Ron Brown* sampled water column chemistry along eight stations across a transect from Galveston, TX, to the open Gulf of Mexico up to 1000 m depth during July 10–12, 2007 (GOMECC-1), and July 31–August 1, 2017 (GOMECC-3) (Table 1). TA, DIC, dissolved oxygen, nutrients (soluble reactive phosphateor or SRP, nitrate + nitrite or NO_x, and silicate), and a host of hydrographic data were collected. To evaluate water carbonate system parameters close to the localized mortality event, we compared the three stations that were at similar latitudes (Fig. 1) to those sampled during the 2016 rapid response cruise, about 120 km west of WFGB. The water depths of these stations were 55 m, 217 m, and 632 m.

For samples collected under the NCRMP and by the CCL, TA was determined using open-cell Gran titration on an alkalinity titrator (Apollo SciTech Inc.), whereas DIC was measured by reacting 0.5 ml samples with 10% phosphoric acid (0.5 M NaCl balanced), and the acid-stripped CO_2 with high-purity N_2 as the carrier gas was quantified using infrared spectrometry on a DIC analyzer (Apollo SciTech Inc.) (Hu et al., 2017). Certified reference material (CRM) obtained from Dr. A. Dickson's lab at the Scripps Institution of Oceanography was used to ensure the proper performance of both the alkalinity titrator and DIC analyzer. Analytical precisions for both TA and DIC analyses were ± 0.1% or better. Purified m-cresol purple (mCP) obtained from Dr. R. Byrne's lab was used to determine the pH of the samples. The absorbance of the indicator was measured at 434 nm and 578 nm at 25 °C in a water-jacketed 10-cm flow cell on an Agilent 8453 spectrometer (Patsavas et al., 2013). The experimental setup was similar to that described in Carter et al. (2013), and the equation in Liu et al. (2011) was used to calculate pH at 25 °C (on total scale) with measurement precision of ± 0.0004. One exception to the above pH analysis was that we used manual dye injection and unpurified mCP for the samples collected in November 2013, and an older version of the pH equation (Clayton and Byrne, 1993) was used for samples collected on that cruise (Table 1).

Analytical methods for the samples collected on the GOMECC-1 cruise can be found in Wang et al. (2013). Briefly, TA was measured using the same open-cell titration, whereas DIC was measured coulometrically (Wanninkhof et al., 2015). For the GOMECC-3 cruise, the same method for DIC analysis was used, whereas TA was measured using a closed-cell titration with certified HCl from Dr. A. Dickson's lab (Wanninkhof et al., 2015). CRM was used periodically to ensure data quality and both measurements had a precison of ± 0.1%. Dissolved oxygen on both GOMECC cruises and the rapid response cruises was measured using Winkler titrations with a ± 0.1% precison (Grasshoff et al., 1999). Apparent oxygen utilization (AOU) was calculated using measured oxygen concentrations and the oxygen solubility as a function of potential temperature and salinity (Weiss, 1970). SRP, NO_x, and silicate from both GOMECC cruises were analyzed at Dr. J.-Z. Zhang's lab

(AOML), with precisions of ± 0.5% (SRP and NO_x) and 1% (silicate) (Zhang et al., 2009, and references therein).

Derived carbonate system parameters (pH, pCO_2, and Ω_{arag} at in-situ temperature and pressure) for the CCL samples were calculated using measured DIC and spectrophotometric pH at 25 °C (Table 1). The MatLab version of the program CO2SYS (van Heuven et al., 2011) was used in all speciation calculations. Carbonate dissociation constants from Mehrbach et al. (1973) refit by Dickson and Millero (1987), the dissociation constant of bisulfate reported in Dickson (1990), the total boron concentration provided in Uppström (1974), and aragonite solubility constant from Mucci (1983) were used in these calculations. In comparison, TA and DIC values were used to calculate the carbonate system parameters of the NCRMP samples because pH was not measured. Carbonate system parameters were calculated using TA, DIC, and nutrients (phosphate and silicate) using the same set of dissociation constants since there was no direct pH measurement (GOMECC-1) or unpurified mCP was used for pH analysis (November 2013 CCL samples, Table 1). To maintain consistency with the GOMECC-1 data, we also used the same input variables (TA, DIC, and nutrients) for speciation calculations of the GOMECC-3 samples (Table 1). Because the differences between the derived carbonate system parameters (pCO_2, in-situ pH, and Ω_{arag}) with and without nutrient input were negligible for oligotrophic surface waters in the Gulf, nutrient data were not used in the carbonate speciation calculations for any of the CCL time-series samples. Note, all pH, pCO_2, and Ω_{arag} presented in this manuscript are values at in-situ conditions.

2.3. CO_2 flux calculation

Air-sea CO_2 flux (F) was calculated using Eq. 1:

$$F = kK_0(pCO_{2w} - pCO_{2a}) \quad (1)$$

where k is gas transfer velocity, K_0 is solubility constant of CO_2 at in-situ seawater temperature and salinity calculated using the equation in Weiss (1974), and pCO_{2w} and pCO_{2a} are partial pressures of CO_2 in surface seawater and the atmosphere, respectively. Global CO_2 record (http://www.esrl.noaa.gov/gmd/ccgg/trends/) was used to calculate pCO_{2a}, using water vapor as a function of surface water salinity and temperature (Weiss, 1974) and assuming one atmosphere pressure. A positive flux means CO_2 degassing from the seawater.

There are a number of k parameterizations in the literature (Prytherch et al., 2010; Wanninkhof, 1992; Wanninkhof et al., 2009; Wanninkhof and McGillis, 1999). Recently, to accommodate future increases in sea surface temperatures to above 30 °C, which the FGBNMS surface water regularly surpassed during our study period, Wanninkhof (2014) used a fourth-order polynomial to fit Sc (i.e., Schmidt number at in-situ temperature, Eq. 2) for the temperature range of −2-40 °C to replace the original third-order fit (Wanninkhof, 1992).

$$k = 0.251 < U^2 > \left(\frac{Sc}{660}\right)^{-0.5} \quad (2)$$

where $< U^2 >$ is the square of wind speed at 10-m height. Thus, we only reported CO_2 flux values based on the latest k formulation in Eq. 2.

Wind speed data were obtained from an ocean buoy located at Station 42,046 (27.890 N 94.037 W) in the FGBNMS region (http://www.ndbc.noaa.gov/station_page.php?station=42046). Whereas wind speed was recorded every 30 min at 3.4 m above the sea surface, the daily wind speed was calculated from the 24-h arithmetic mean of the anemometer readings and then converted to speed at 10 m height using the relationship presented in Hsu et al. (1994).

2.4. Data interpolation

To examine decadal changes in both the carbonate system parameters and other biogeochemical data (i.e., oxygen and nutrients) in subsurface waters, these data were interpolated onto individual potential density surfaces at 0.1 intervals using piecewise cubic interpolation in MatLab (σ_θ = 26.1–26.7, corresponding to water depth of ~100–250 m).

2.5. Multilinear regression

Given that nutrient concentrations were close to zero in surface waters, we examined the controls on surface water carbonate system parameters (pH, Ω_{arag}, and pCO_2) using multilinear regression (MLR) based on available field data including sea surface temperature (SST) and salinity (SSS). To find the best-fit models for these parameters, we used the statistical package *MuMIn* (https://cran.r-project.org/web/packages/MuMIn/index.html) and *Car* (https://cran.r-project.org/web/packages/car/index.html) on the open source platform R Studio (Ver 1.1.383). A stepwise, exhaustive search of linear models using the function *Dredge* (in the package *MuMIn*), in combination with the function *Vif* (in the package *Car*), was employed by identifying model fits with the lowest second order Akaike Information Criterion (AICc) (Burnham and Anderson, 2002), while the Variance Inflation Factor (VIF) was used to detect collinearity (VIF value < 5) (Kutner, 2004). Basically, these steps evaluated the MLR model fits with SST, SSS, or a combination of both. The chosen linear model had to pass both the Shapiro-Wilk test (for residual normality) and the Breusch-Pagan test (for homoscedasticity) to meet all assumptions of a linear model (using the criterion $p > 0.05$).

3. Results

3.1. Internal consistency

Based on the samples for which pH was measured using purified mCP at 25 °C (2014–2016), the residual between calculated and measured TA (i.e., $\Delta TA = TA_{meas} - TA_{cal'd}$) was 1.6 ± 10.9 μmol kg^{-1} (n = 91, Table S1), similar to results from a recent study that also examined Gulf of Mexico coastal waters (e.g., Patsavas et al., 2015) but with slightly higher standard deviation of the residuals (10.9 μmol kg^{-1} in this study vs. ~7 μmolg kg^{-1} in Patsavas et al., 2015). However, the residual for the November 2013 data was 25.9 ± 6.4 μmol kg^{-1} (n = 8), indicating a bias caused by the dye impurity that led to underestimated pH values (Liu et al., 2011). Therefore, in-situ pH, Ω_{arag}, and pCO_2 for this cruise were calculated solely based on TA and DIC (Table 1). In the 2016 rapid-response cruise, calculated TA was 1.6 ± 6.4 μmol kg^{-1} (n = 34) lower than the measured values. Given that nutrient data were not available for the rapid response cruise, and nutrients would slightly contribute to TA in subsurface waters, ΔTA could be lower than 1.6 μmol kg^{-1}. For example, if phosphate and silicate concentrations were 1 μmol kg^{-1} and 10 μmol kg^{-1} throughout the water column during the rapid response cruise, the maximum values found in the upper 250 m of the three GOMECC-1 stations, ΔTA would decrease to ~0.1 μmol kg^{-1}. On the other hand, calculated pH, pCO_2, and Ω_{arag} from the rapid response cruise (pH, DIC) pair with and without the same nutrient concentrations as above differed by 10^{-5} pH units, 10^{-2} μatm, and 10^{-4}, respectively, all significantly lower than the respective standard deviations of residuals due to the selection of different carbonate parameters as input pairs (e.g., Table 2, also see next paragraph).

Different input pairs, i.e., the (DIC, TA) pair vs. the (pH, DIC) pair for the FGBNMS time-series study and the (DIC, TA) pair vs. (DIC, pCO_2) pair for the GOMECC-1 study, generated substantial standard deviations of residuals for the derived parameters (pH, Ω_{arag}, and pCO_2, Table 2). For example, using the (DIC, TA) pair vs. the (pH, DIC) pair from the FGBNMS dataset, standard deviations of residuals for pH and Ω_{arag} were 0.014 pH units and 0.107, respectively, despite that the mean values for both parameters were close to zero (Table 2). On the other hand, using the (DIC, TA) pair vs. the (DIC, pCO_2) pair from the

Table 2
Differences in in-situ pH, Ω_{arag}, and pCO_2 calculated using different pairs of measured parameters for the FGBNMS time-series samples. Note the input pH were measured at 25 °C and input pCO_2 was measured at 20 °C.

Residual	Mean	SD	Max Δ	Min Δ
FGBNMS time-series				
pH(DIC, TA) – pH(pH, DIC)	0.0005	0.0139	0.0380	−0.0376
Ω_{arag}(DIC, TA) – Ω_{arag}(pH, DIC)	0.001	0.107	0.275	−0.301
pCO_2(DIC, TA) – pCO_2(pH, DIC) (μatm)	−0.3	14.4	42.5	−35.0
GOMECC-1 (stations shown in Fig. 1)				
pH(DIC, TA) – pH(DIC, pCO_2)	−0.0142	0.0131	0.0088	−0.0378
Ω_{arag}(DIC, TA) – Ω_{arag}(DIC, pCO_2)	−0.075	0.071	0.075	−0.176
pCO_2(DIC, TA) – pCO_2(DIC, pCO_2) (μatm)	17.1	17.2	51.3	−8.4

GOMECC-1 dataset, standard deviations of residuals for pH and Ω_{arag} were slightly smaller than for the FGBNMS study but that for Ω_{arag} was consistent with an earlier study (Patsavas et al., 2015), although the mean residuals were much larger (−0.075 in Table 2 vs. -0.014 in Patsavas et al., 2015). Because only the quality-controlled DIC, TA, and nutrient data from the GOMECC-3 study were available at the time of preparing this manuscript, we did not perform internal consistency calculations for this dataset. Given the good internal consistency of the 2016 rapid response cruise and negligible influence of nutrient on the speciation calculations for pCO_2, Ω_{arag} and pH, the (pH, DIC) pair was used for subsurface water speciation calculations. The results were compared with the two GOMECC datasets derived using the (TA, DIC) pair and nutrients.

3.2. Temporal variations in surface water at the three FGBNMS sites

Salinity at FGBNMS sites stayed within a narrow range (35.5–36.7) throughout our sampling period, except after a flood caused by extreme rainfall events in Texas and Louisiana in summer 2016. As a result, surface salinity in August decreased to as low as 33.9 (Fig. 2a, Table 3). In comparison, SST showed a clear seasonal variation ranging from ~20–30 °C, and this seasonal variation can be approximately represented by a harmonic function of time (Fig. 2b).

Similar to salinity, TA and DIC in the surface water exhibited small variations, i.e., 2340–2415 μmol kg^{-1} (average 2391 ± 19 μmol kg^{-1}) and 2015–2092 μmol kg^{-1} (2060 ± 19 μmol kg^{-1}), respectively (Table 3). Both TA and DIC reached their respective minimum values of 2340 μmol kg^{-1} at SB in May 2016 and 2015 μmol kg^{-1} at EFG in August 2016, after a period of extensive continental flooding. By excluding data from the two cruises that captured a relatively large salinity decreases, the TA variability would be substantially reduced, with TA averaging 2397 ± 8 μmol kg^{-1}, while no significant change to DIC was observed (2068 ± 16 μmol kg^{-1}).

Calculated in-situ pH (based on measured pH at 25 °C and DIC) ranged between 8.006 and 8.115, Ω_{arag} ranged between 3.417 and 4.164, and pCO_2 ranged between 340 and 455 μatm across all three banks (Table 3 and Fig. 3). In August 2016, pH reached 8.006 at SB, the lowest value in the three-year time-series of the CCL data (but note that values as low as 7.948 appeared in the NCRMP data, Fig. 3a), and pCO_2 reached maximum values (449 ± 6 μatm, Fig. 3c). Conversely, the highest surface water pH (8.109 ± 0.005, Fig. 3a) was measured in February 2015 and corresponded to the lowest pCO_2 (346 ± 6 μatm, Fig. 3c) across all three sites (also see Table 3).

Maximum seawater CO_2 uptake (−4.17 ± 0.83 mmol-C m^{-2} d^{-1}) was observed in February 2016, and maximum CO_2 degassing (7.62 ± 0.78 mmol-C m^{-2} d^{-1}) was observed in August 2016 (Fig. 4). A simple average of all calculated daily CO_2 flux values yielded 0.61 ± 2.80 mmol-C m^{-2} d^{-1}, and if both May and August 2016 data were removed as this period was substantially influenced by flooding, the average value becomes −0.14 ± 1.96 mmol-C m^{-2} d^{-1}.

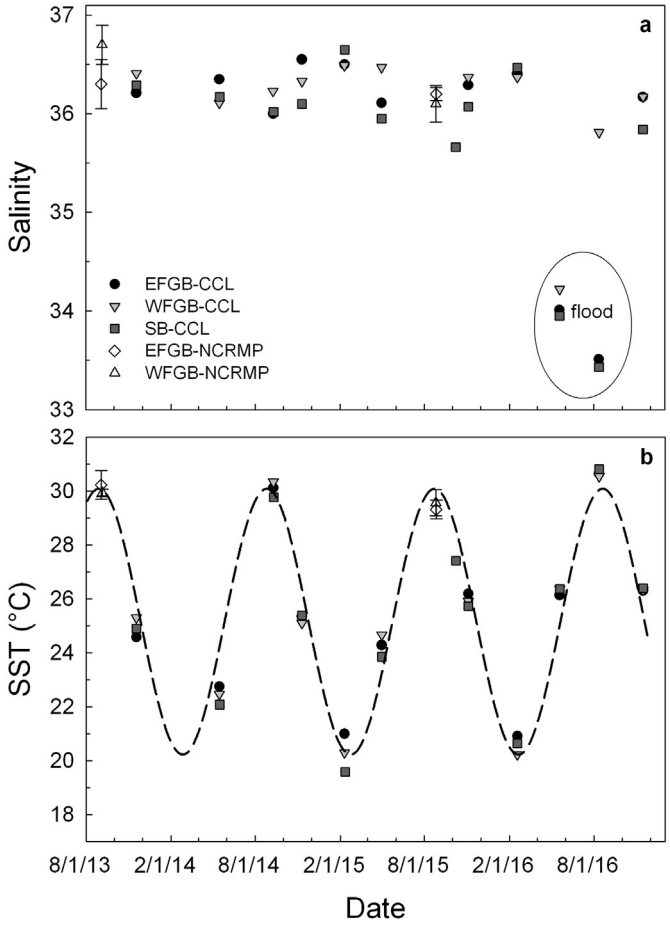

Fig. 2. Sea surface salinity (SSS, a) and temperature (SST, b) in 2013–2016. CCL represents Carbon Cycle Lab, and NCRMP represent National Coral Reef Monitoring Program. NCRMP had multiple sample collections on each day of visit, only the average data are shown and the error bar represents standard deviation of the mean. Dashed curve in (b) represents a harmonic fit to the SST.

3.3. Depth variation of the water column carbonate system parameters at FGBNMS sites

Throughout 2013–2016, there was little water column stratification at all three FGBNMS sites with bottom-surface salinity and temperature differences < 2.1 and < 1.8 °C, respectively. Maximum stratification was observed during flooding in May 2016, consistent with the largest bottom-surface TA and DIC differences. For example, bottom-water TA and DIC in May 2016 were respectively ~50 μmol kg^{-1} and 30 μmol kg^{-1} greater than the surface water values at both SB and WFG, while the differences were smaller at EFG (30 μmol kg^{-1} and 20 μmol kg^{-1}, respectively). Overall, there was no significant difference between surface and bottom waters during the entire sampling period (paired *t*-test, $p > 0.05$). Similarly, the differences in pH and Ω_{arag} between bottom and surface waters (i.e., bottom-water value - surface-water value) also were not significant during this period (paired t-test, $p > 0.05$). Maximum bottom-surface pH and Ω_{arag} differences were observed in May 2016 at WFGB, and bottom-water pH and Ω_{arag} were 0.013 and 0.021 higher than those in the surface water, respectively. This largest bottom-surface difference coincided with the maximum salinity stratification at this location (bottom-water salinity was 2.1 higher), as the lower pH and Ω_{arag} reflected freshwater influence at the surface. Nevertheless, the narrow ranges of the carbonate system parameters (69 μmol kg^{-1} for TA, 80 μmol kg^{-1} for DIC, 0.14 pH units and 0.79 for Ω_{arag}, respectively, Fig. 5) indicate a relatively stable seawater carbonate system in this outer shelf region.

Table 3
Average temperature, salinity, TA, DIC, and pH, Ω_{arag}, and pCO_2 under in-situ conditions in the surface water of the FGBNMS sites in 2013–2016. Uncertainties are one standard deviation of the mean, and values in parentheses are ranges.

Site	T (°C)	Salinity	TA (μmol kg^{-1})	DIC (μmol kg^{-1})	pH	Ω_{arag}	pCO_2 (μatm)	n
EFGB	25.30 ± 3.16 (20.91–30.65)	35.95 ± 0.97 (33.89–36.63)	2388.4 ± 20.0 (2344.5–2408.6)	2058.5 ± 21.8 (2015.5–2091.6)	8.064 ± 0.027 (8.014–8.103)	3.711 ± 0.218 (3.428–4.164)	388.9 ± 28.4 (351.8–442.5)	11
WFGB	25.24 ± 3.39 (20.23–30.55)	36.18 ± 0.61 (34.46 ± 36.70)	2395.7 ± 13.7 (2357.4–2409.8)	2063.2 ± 14.1 (2048.0–2085.7)	8.066 ± 0.032 (8.008–8.109)	3.738 ± 0.249 (3.433–4.171)	387.9 ± 33.9 (345.0–450.3)	11
SB	25.28 ± 3.52 (19.59–30.81)	35.82 ± 0.94 (34.07–36.65)	2387.6 ± 23.0 (2339.7–2415.3)	2059.2 ± 21.6 (2026.6–2087.8)	8.065 ± 0.032 (8.006–8.115)	3.657 ± 0.195 (3.417–3.863)	388.3 ± 32.8 (339.8–454.6)	10

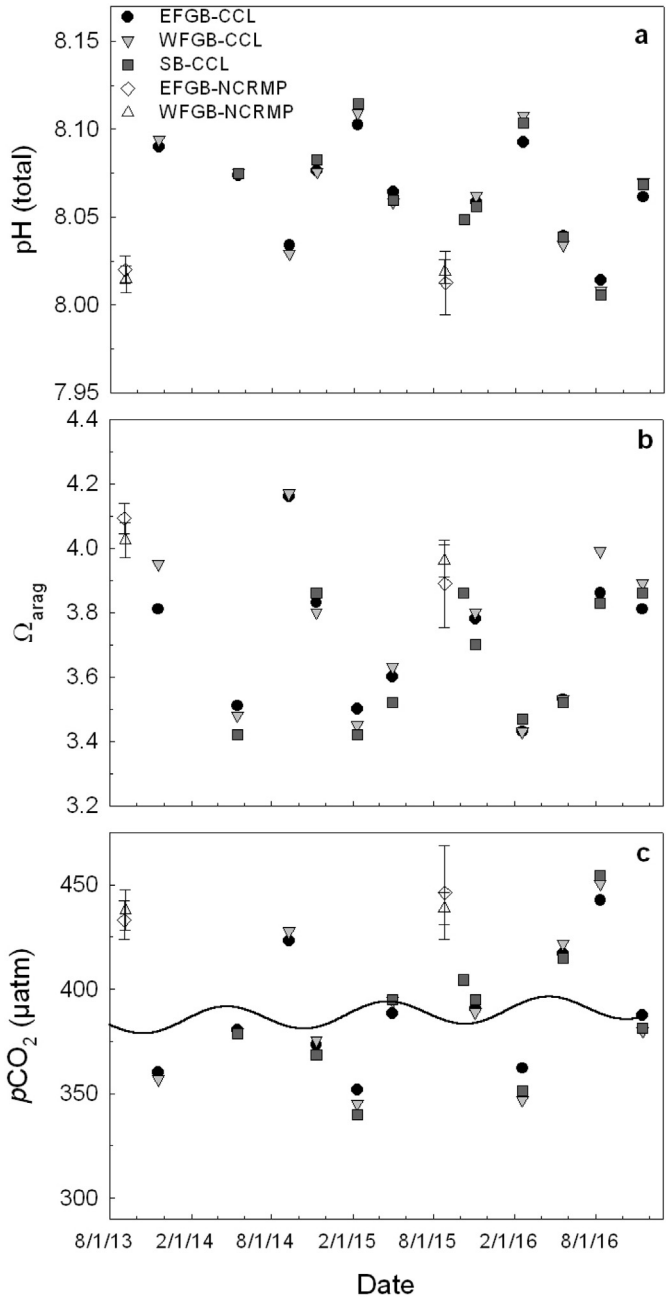

Fig. 3. Sea surface pH (a), Ω_{arag} (b), and pCO_2 (c) in 2013–2016 at in-situ conditions. The solid curve in panel c represents the atmospheric pCO_2, which was calculated using the global atmospheric CO_2 record (http://www.esrl.noaa.gov/gmd/ccgg/trends/), a harmonic-fit of SST (Fig. 2), and a harmonic fit of water vapor as a function of salinity and temperature (Weiss, 1974). One atmosphere pressure was assumed in this calculation.

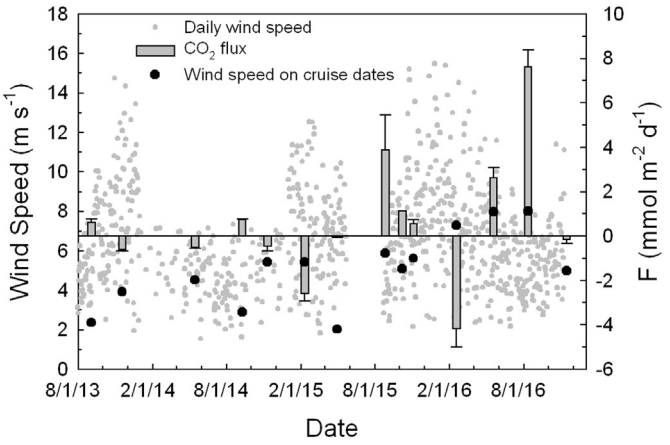

Fig. 4. Air-sea CO_2 flux at the FGBNMS region. The grey circles are daily wind speed at 10 m height, and the black circles are wind speed on the cruise dates. Error bar represents standard deviations of CO_2 flux calculated from average of the three locations (for CCL samples) and average of multiday measurements (for NCRMP samples) (Table 1). Positive flux means CO_2 degassing from seawater.

3.4. Relationship between SST, SSS and surface-water carbonate system parameters

Based on surface water data from all seasonal cruises during the 2013–2016 period, both SST and SSS were significant independent variables in MLR models with no collinearity (VIF < 5) for the four carbonate system parameters (DIC, pH, Ω_{arag}, and pCO_2), whereas SSS is the only predicator variable in the best model for TA (Table 4). Samples from May and August 2016 cruises (Table 1) had the lowest salinity compared with the rest of the sampling period (Fig. 2). If the data from these two cruises were excluded, neither SST nor SSS displayed a significant linear relationship with TA, and the best fit models for DIC, pCO_2, and pH incorporated only SST as a predicator variable in the linear regression (Table 4). Nevertheless, SSS remained a significant predictor variable for Ω_{arag} based on AICc, although using SST alone in a simple linear model for Ω_{arag} only marginally reduced R^2 from 0.908 to 0.880 and increased the standard error from 0.070 to 0.080 (Table 4). Likewise, using SST alone as the sole predictor also generated significant results for DIC, pH, and pCO_2 for the entire dataset as well as when the flooding influence was removed. These simpler regressions also passed the significance tests ($p << 0.001$, Fig. 6), indicative of the dominant temperature control on carbonate system parameters in FGBNMS waters.

3.5. Changes in carbonate system parameters on decadal timescale

The potential temperature (θ) and salinity diagram (T-S) indicates that the upper water column (< ~100 m or potential density σ_θ < 26.1) in the FGBNMS region had significant interannual variability over the period of 2007–2017 (Fig. 7). To examine decadal changes in the carbonate system parameters based on the three

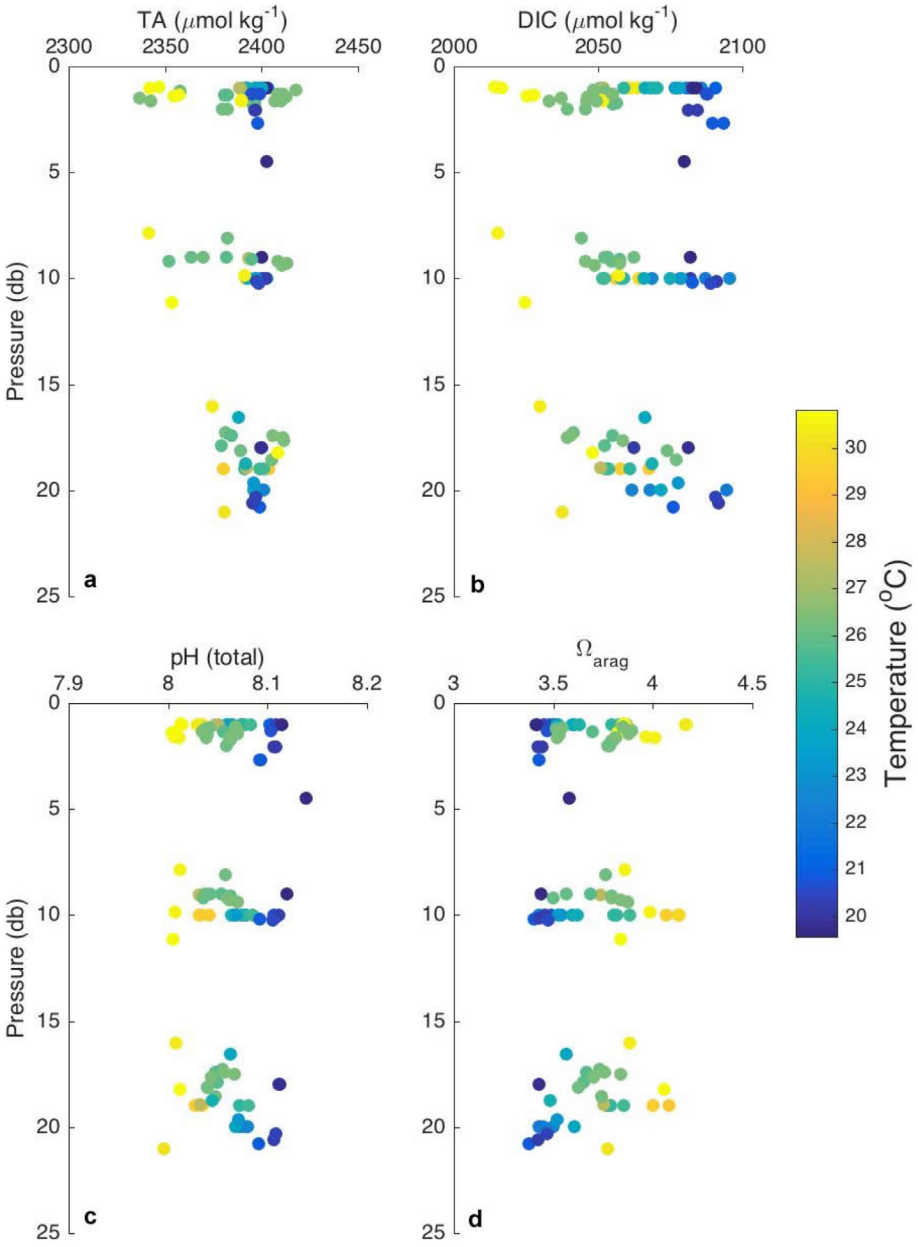

Fig. 5. Depth distributions of TA, DIC, in-situ pH, and in-situ Ω_{arag} during the 2013–2016 period. Note db (decibar) is numerically similar to meter in shallow continental shelf waters. Colorbar represents temperature. (For interpretation of the references to colour in this figure legend, the reader is referred to the web version of this article.)

"snapshot" cruises, this upper water column was therefore omitted. On the other hand, since the 2016 rapid response cruise only sampled up to 241 m depth (or 242.5 db, σ_θ < 26.8), we limited our data interpretation to the upper 250 m for the two GOMECC cruises. The physical conditions of the ~100–250 m water column appeared to have remained similar (Fig. 7).

Both physical (pressure, salinity, θ) and chemical parameters (TA, DIC, AOU, NO_x, and SRP, in-situ pH, Ω_{arag}) of the three cruises were interpolated on individual potential density surfaces (σ_θ = 26.1–26.7) at 0.1 intervals. Standard deviations (SD) of hydrostatic pressure, salinity, and θ of each isopycnal ranged between 10 and 20 db, 0.006–0.054, and 0.02–0.29 °C, respectively, and that for TA was largely within analytical uncertainty (< 2.2 μmol kg^{-1}) except at σ_θ = 26.7, where SD = 4.2 μmol kg^{-1} (Fig. 8). The small changes in salinity, θ and especially TA suggest that the examined depth range did not exhibit significant changes, at least during the three separate cruises that spanned a 10-year period.

In contrast to the stable TA and physical conditions, nutrients, AOU, DIC, and the derived in-situ pH and Ω_{arag} all exhibited noticeable changes throughout the examined depth range (Fig. 9). When the 2007 and 2017 datasets were compared, the largest changes were seen at the topmost isopycnal surface (i.e., σ_θ = 26.1), where AOU and DIC increased by 53 and 45 μmol kg^{-1}, respectively (Table 5). At the same time, pH and Ω_{arag} at σ_θ = 26.1 decreased by 0.090 pH units and 0.453, respectively (Fig. 9). At the lowest isopycnal (σ_θ = 26.7), AOU and DIC both increased 10 μmol kg^{-1} (Table 5), while pH and Ω_{arag} decreased 0.041 pH units and 0.163, respectively (Fig. 9). In comparison, the differences of these parameters between the 2016 and 2017 cruises were much smaller and the changes were only noticeable within the isopycnal 26.1–26.5 (~100–150 m) (Fig. 9).

Table 4
Regression analysis of the controlling factors on surface water carbonate parameters in FGBNMS.

	Dependent variable	Fitting variable	VIF	R^2	Standard error
All data	TA	SST[a] SSS	1.43, 1.43	0.806	8.59
		SSS		0.797	8.65
	DIC	SST SSS	1.43, 1.43	0.720	10.35
		SST		0.655	11.30
	pH	SST SSS	1.43, 1.43	0.877	0.011
		SST		0.812	0.013
	Ω_{arag}	SST SSS	1.43, 1.43	0.905	0.070
		SST		0.670	0.127
	pCO_2	SST SSS	1.43, 1.43	0.859	11.94
		SST		0.778	14.71
Data w/o flooding influence	TA	SST[a], SSS[a]	1.44, 1.44	0.003	7.812
		–	–	–	–
	DIC	SST SSS[a]	1.44, 1.44	0.586	10.71
		SST		0.584	10.51
	pH	SST SSS[a]	1.44, 1.44	0.789	0.011
		SST		0.763	0.011
	Ω_{arag}	SST SSS	1.44, 1.44	0.908	0.070
		SST		0.880	0.080
	pCO_2	SST SSS[a]	1.44, 1.44	0.745	11.82
		SST		0.717	12.18

[a] indicates non-significant predictor variable for the MLR model ($p > 0.05$).

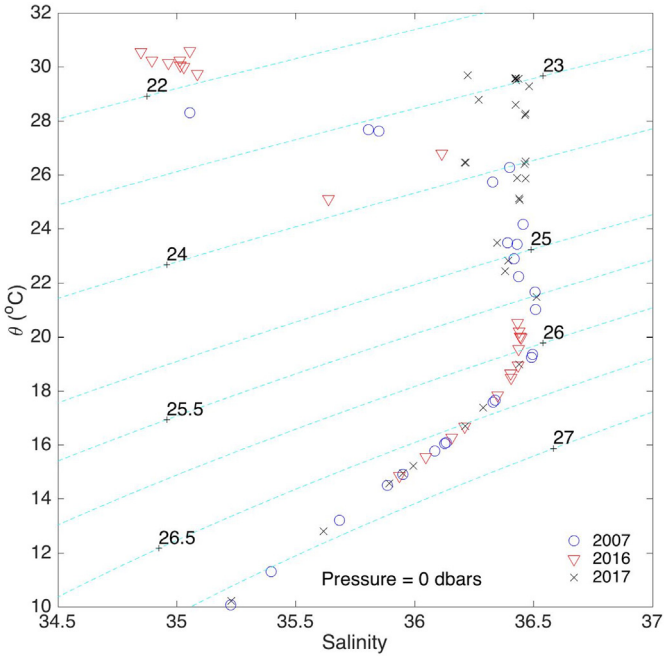

Fig. 7. T-S diagram of the 2007 GOMECC-1, 2016 rapid response, and 2017 GOMECC-3 cruises at the sampling stations shown in Fig. 1. The contour lines represent isopycnals (kg m^{-3}) at reference pressure 0 bar.

4. Discussion

4.1. Controlling factors of carbonate system parameters at the FGBNMS sites

FGBNMS is different from typical shallow water reefs in the nearby Caribbean Sea as it is deep (20 m or more) and small in areal extent relative to other coral reefs. Since we did not observe diel changes in this study as the sampling occurred about once per quarter, we only interpreted the seasonal changes in the context of larger scale seawater carbonate system parameters in subtropical regions.

When there was little terrestrial freshwater runoff (excluding May and August 2016), salinity only ranged between 35.8 and 36.7 (Fig. 2a), and no significant correlation was found between TA and salinity ($p > 0.05$, Table 4). Nevertheless, a significant linear relationship emerged between TA and salinity from the upper 20 m water column that was surveyed in the broader FGBNMS region from May and August 2016 (TA = (25.20 ± 0.47)S + (1490.0 ± 16.1), Fig. 10, also see Table 4). During this time the continental flooding influence persisted and the FGBNMS sites experienced noticeable freshening. The intercept of this regression was 1490 ± 16 μmol kg^{-1}, and this non-zero intercept indicates that the salinity decrease in the FGBNMS region was not due to a local precipitation event, which would have generated a zero-intercept on the TA-salinity plot. Rather, it represented distal freshwater input from the land. Even though this y-intercept shows that considerable mixing had taken place despite the narrow seawater salinity range examined here (31.6–36.4, Fig. 10), the apparent freshwater endmember appeared to correspond to river waters of moderate

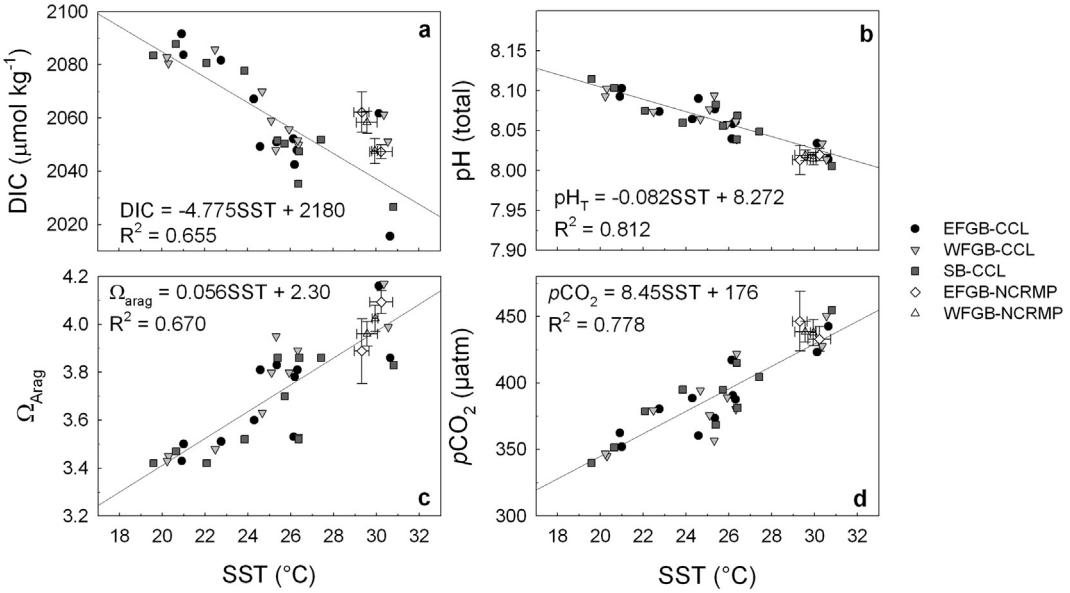

Fig. 6. Relationships between surface water DIC, pH, Ω_{arag}, and pCO_2 and sea surface temperature (SST). The data points with error bars were collected in early September 2013 and late August 2015 by NCRMP (Manzello, unpublished).

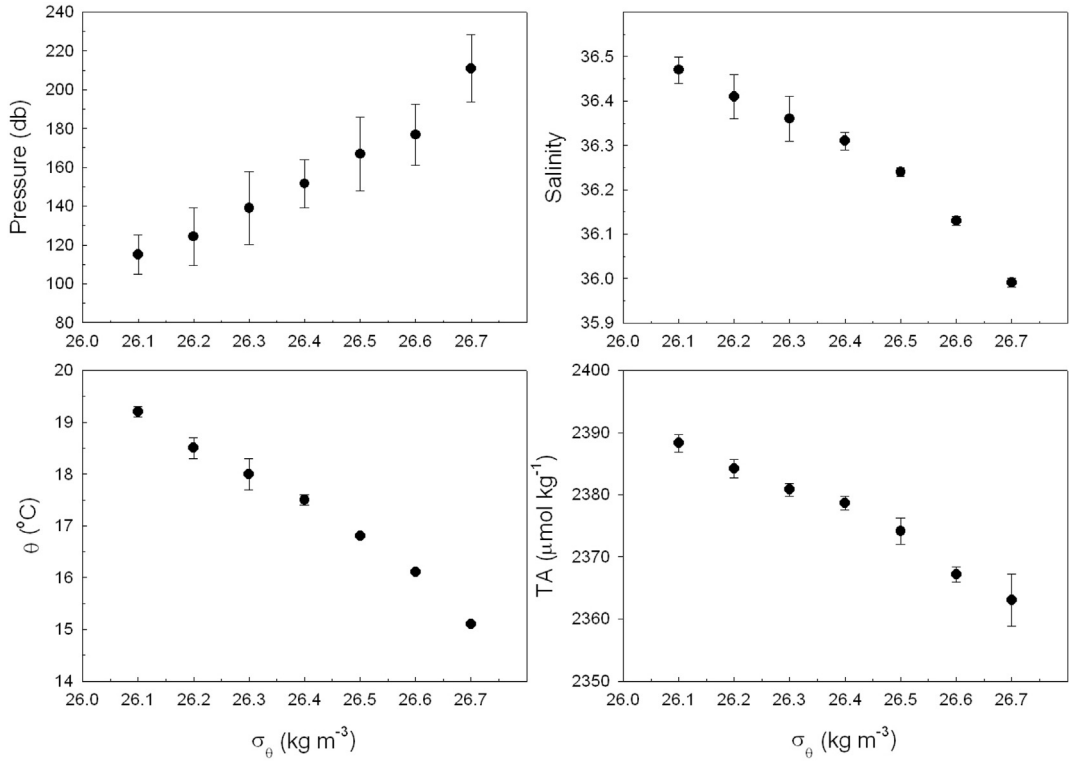

Fig. 8. Interpolated hydrostatic pressure, salinity, potential temperature, and TA on individual isopycnal surfaces (σ_θ).

TA levels found in northern Gulf along the coast of Texas and Louisiana (Hu et al., 2015; Huang et al., 2015a).

The fact that temperature was a significant predictor variable for DIC, pH, Ω_{arag}, and pCO_2 (Table 4) suggests that seasonal temperature fluctuations were important in controlling CO_2 equilibria in these waters, given that TA had a narrow range (2397 ± 8 μmol kg^{-1}, Section 3.2) except during the period that was affected by flooding. Therefore, it is worth exploring the extent of temperature control vs. other possible factors on the seawater CO_2 system.

In the literature, sea-surface pCO_2 data are often normalized to an average temperature across observational windows to remove the temperature effect and examine the relationship between CO_2 variability and biological activity (Takahashi et al., 2002; Takahashi et al., 2009). Using the equation in Takahashi et al. (2002), we first normalized pCO_2 in surface water to the average SST (25.3 °C) using the $\partial \ln pCO_2/\partial T$ value of 0.0404 calculated for FGBNMS waters, which is slightly lower than the literature value 0.0423 (Takahashi et al., 2002), and the temperature-normalized pCO_2 ($npCO_2$) showed a significantly negative relationship with SST (data not shown), indicating increased production at higher temperature. There was a net 84 μatm $npCO_2$ decrease from winter to summer that can be attributed to a combination of biological activity and air-sea exchange (Takahashi et al., 2002) as well as terrestrial freshwater influence, which presumably could have delivered nutrient to this oligotrophic area and caused episodic surface production. To examine the net thermal effect on pCO_2 variations, we used the average surface pCO_2 value (388 μatm) and calculated the effect of the observed temperature span (19.6–30.8 °C). The result indicates that pCO_2 ranged between 309 and 486 μatm as a result of temperature change only, a net difference of 177 μatm. Clearly, the thermal effect (177 μatm) on pCO_2 variability far outweighed biological effects (84 μatm) in FGBNMS waters.

In the FGBNMS region, pCO_2 variations caused by temperature and biological effects were both greater than those reported for the Bermuda Atlantic Time Series (BATS) (32°50′N and 64°10′ W) (Takahashi et al., 2002), a well-studied area that is also located in the North Atlantic Ocean. Temperature fluctuations are slightly smaller at BATS (~19–29 °C), which leads to a ~150 μatm seasonal pCO_2 variation. The biologically-induced change in pCO_2 is only 55 μatm (vs. 84 μatm at FGBNMS). The dominant temperature effect on pCO_2 changes also led to significant relationships between temperature and pH as well as Ω_{arag} (Fig. 6), since surface TA was stable across the sampling period (mean ± standard deviation: 2398 ± 7 μmol kg^{-1}, $n = 27$) when the data affected by continental flooding were excluded. Compared to the oligotrophic ocean gyre where BATS is located (Bates, 2017; Johnston et al., 2017b), the FGBNMS area had greater nutrient supply due to its closer proximity to the continent where large rivers are often nutrient-enriched (Rabalais et al., 2014), despite nutrient concentrations were often being below detection limits, which would explain the greater biological effect on seasonal pCO_2 variations. For example, the surface water nitrate level at BATS was never above 2 μmol kg^{-1} (http://batsftp.bios.edu/BATS/bottle/), while at the FGBNMS sites nitrate can be as high as 11.4 μmol kg^{-1} based on historical data (Johnston et al., 2017b).

4.2. Seawater pCO_2 and CO_2 flux implications in the FGBNMS region

A comparison between the atmospheric pCO_2 and sea-surface pCO_2 suggests that the largest sea-to-air pCO_2 gradient occurred in summer (ΔpCO_2, ~50–70 μatm), especially under the influence of flooding; seawater pCO_2 was lowest in late winter with ΔpCO_2 of −40~ − 45 μatm. In all other seasons, ΔpCO_2 was mostly within ± 10–20 μatm of the atmospheric value. Despite the sparse data coverage, integrated ΔpCO_2 largely cancelled out on an annual basis. For example, the average sea-surface pCO_2 over the three-year period was 388 ± 31 μatm ($n = 32$), compared to the atmospheric pCO_2 level of 387 ± 5 μatm. By removing the 2016 data that were influenced by the flooding event (May and August), the average seawater pCO_2 becomes 378 ± 23 μatm (n = 27).

According to ΔpCO_2 (Fig. 3c), CO_2 uptake mostly occurred in cold months and release occurred in warm months (Fig. 4), but the magnitude of CO_2 flux (both uptake and release) appeared to become higher after the latter half of 2015. This increase can be attributed to both

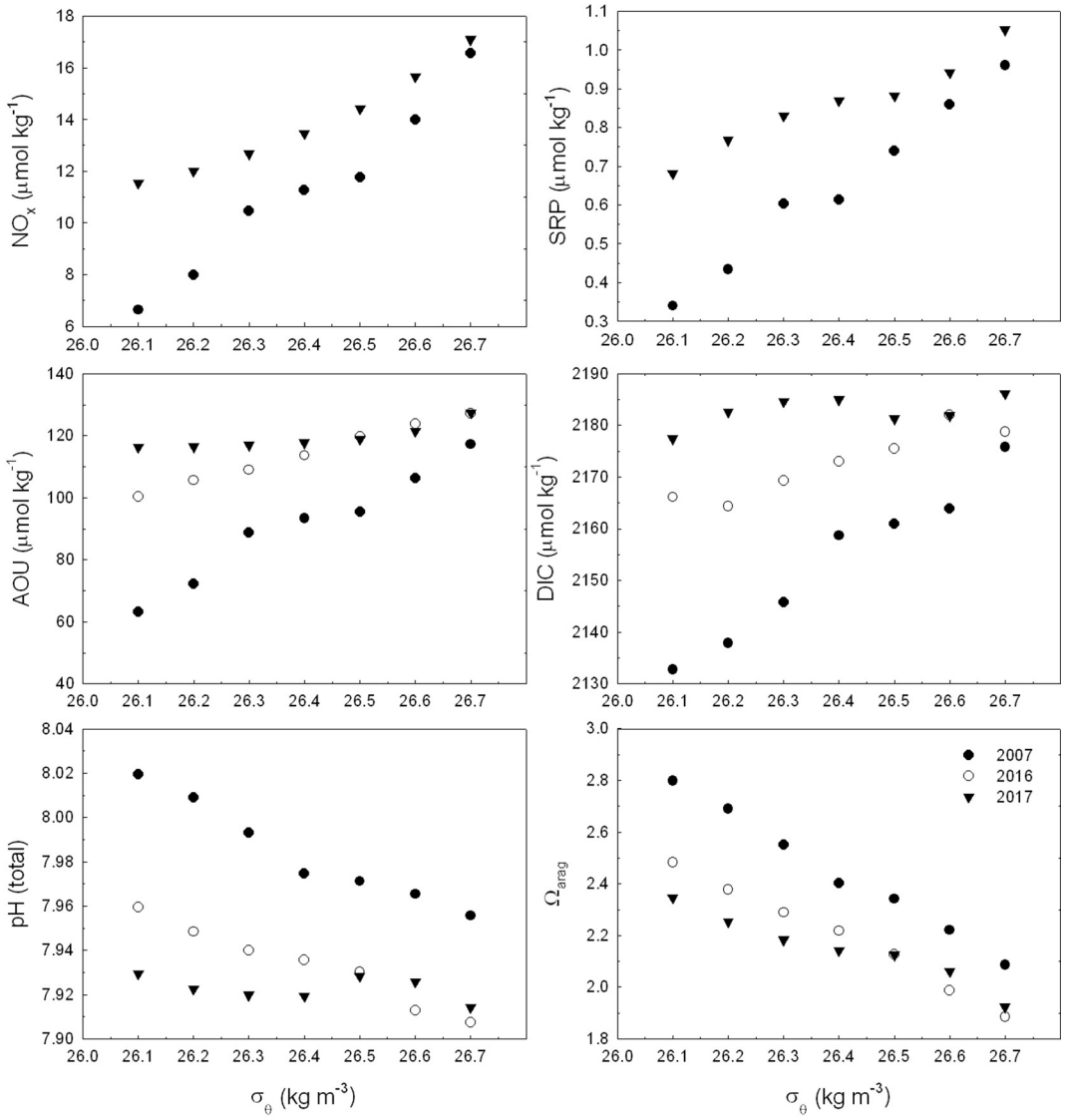

Fig. 9. Interpolated water column nutrients (nitrate + nitrite or NO_x, soluble reactive phosphate or SRP), apparent oxygen utilization (AOU), DIC, pH, and Ω_{arag} on individual isopycnal surfaces (σ_θ).

higher pCO_2 and higher wind speed during the latter cruises. The highest CO_2 efflux observed in August 2016 likely suggests floodwater-induced shelf water degassing due to degradation of riverine organic matter at high seawater temperatures (> 30.5 °C at all three sites). Nevertheless, the slightly negative average CO_2 flux (-0.14 ± 1.96 mmol-C m^{-2} d^{-1}, Section 3.2, but note the large uncertainty), if the episodic floodwater influence is ignored, suggests that these waters could be a weak CO_2 sink during "normal" years, although a change in freshwater input from the land during a short period of time could easily tilt the mass balance. Furthermore, the overall CO_2 flux value (without flood influence) is similar to that in the open northern Gulf of Mexico at a salinity range of 35–37 (i.e., -0.1 ± 2.0 mmol-C m^{-2} d^{-1}, Huang et al., 2015b).

These results are consistent with the notion that this area is mostly

Table 5
Ratios of AOU and nutrient concentration changes between 2007 and 2017 and estimated anthropogenic CO_2 in the water column based on various reaction stoichiometry.

σ_θ	ΔAOU	ΔDIC	ΔP	ΔN	ΔAOU/ΔP	ΔAOU/ΔN	ΔN/ΔP	$C_{ant\_Redfield}$ (μmol kg^{-1})	C_{ant_Xue} (μmol kg^{-1})
26.1	53.2	44.6	0.34	4.91	155.3	10.8	14.3	8.0 ± 4.2	13.8 ± 4.1
26.2	44.3	44.7	0.33	4.03	132.5	11.0	12.1	12.7 ± 4.7	17.7 ± 4.1
26.3	28.2	38.8	0.23	2.22	124.4	12.7	9.8	18.7 ± 4.9	21.9 ± 4.2
26.4	24.4	26.3	0.26	2.21	95.4	11.0	8.6	6.1 ± 6.4	9.4 ± 5.2
26.5	23.5	20.4	0.14	2.67	164.0	8.8	18.6	3.4 ± 1.6	6.1 ± 1.5
26.6	15.2	18.0	0.08	1.68	185.9	9.1	20.5	7.5 ± 1.6	9.2 ± 1.5
26.7	10.1	10.4	0.09	0.54	109.4	18.9	5.8	3.3 ± 3.2	4.5 ± 2.7
Mean	28.4	29.0	0.21	2.61	138.1	11.8	12.8	8.5	11.8
SD	15.4	13.7	0.11	1.46	31.9	3.4	5.4	5.5	6.3

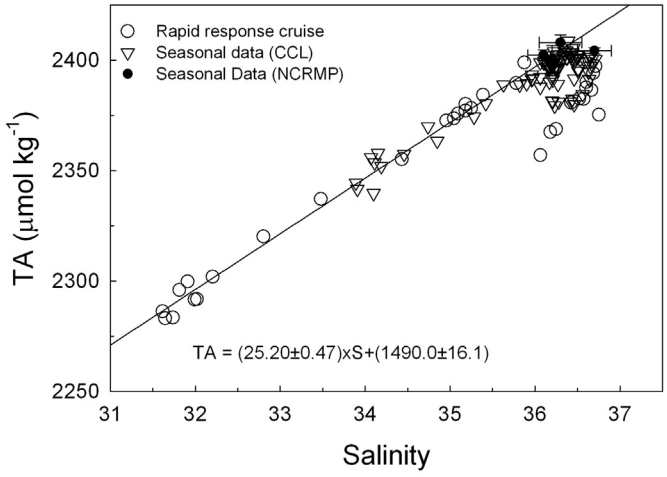

Fig. 10. TA vs. salinity from the FGBNMS sites during the 2013–2016 period and the rapid response cruise in August 2016. The regression uses the May and August seasonal cruise data from the three FGBNMS sites and the upper 20 m water column data from the rapid response cruise.

oligotrophic and physical control (mostly temperature) played an important role in regulating seawater pCO_2 variations, whereas significant continental flooding can bring high pCO_2 water and possibly terrestrial organic carbon and cause ephemeral CO_2 degassing in this outer shelf region. With continuing CO_2 increase in the atmosphere, it is also likely that seawater here will further take up CO_2, resulting in a progressive accumulation of this greenhouse gas in the surface water.

4.3. Controls on decadal subsurface carbonate system parameter changes

To the best of our knowledge, despite a number of studies that examined "snapshots" of carbonate system parameters in the northern Gulf of Mexico (e.g., Wang et al., 2013; Wanninkhof et al., 2015), no study has investigated decadal variability. Data from the 2007 GOMECC-1 cruise, the rapid-response cruise in early August 2016, and the 2017 GOMECC-3 cruise offer a good opportunity to do so.

In the literature, isopycnal surfaces have been used to examine anthropogenic CO_2 accumulation in ocean basins (Lee et al., 2003; Peng and Wanninkhof, 2010; Sabine et al., 2002; Wanninkhof et al., 2010). Even though there were limited data in this outer shelf region, given the stable physical conditions in the ~100–250 m depth range during the three cruises (Fig. 7), interpreting the changes in chemical signals may offer valuable insights on the decadal changes in water column biogeochemical conditions.

The apparent pH and Ω_{arag} decrease (Fig. 9) over the 10-year period (2007–2017) in the ~100–250 m depth range, i.e., 0.041–0.090 pH units and 0.163–0.453, appear to be greater than those reported in open ocean waters. For example, surface water pH decrease rates range from 0.0017 to 0.0021 yr^{-1} in different ocean basins (Byrne et al., 2010; González-Dávila et al., 2007; Woosley et al., 2016), and the Ω_{arag} decrease rate is 0.012 ± 0.001 yr^{-1} in the adjacent Caribbean Sea (Gledhill et al., 2008).

The greater acidification signal in the subsurface waters was in part due to excess respiration because AOU, DIC, and nutrient concentrations were all elevated in 2017 compared to 2007 (Fig. 9). Using the interpolated data along the selected isopycnal surfaces, apparent reaction stoichiometry between oxygen, carbon and nutrients were calculated (Table 5). As anthropogenic CO_2 uptake (C_{ant}, without nutrient changes) is separate from CO_2 production due to respiration in the water column (with nutrient changes), it was possible to estimate the fraction of C_{ant} contribution based on the respiration signals and reaction stoichiometry. The most used Redfield composition of marine produced organic matter has the formula of $(CH_2O)_{106}(NH_3)_{16}(H_3PO_4)$ (Redfield, 1934; Redfield, 1958). Thus, a complete aerobic respiration would generate ΔAOU:ΔDIC:ΔN:Δ*P* = 138:106:16:1. Individual ratios (Table 5) calculated using the interpolated data, i.e., ΔAOU/ΔN (11.8 ± 3.4), ΔAOU/ΔP (138.1 ± 31.9), and ΔN/ΔP (12.8 ± 5.4), were all consistent with the Redfield reaction stoichiometry (*t*-test, $p > 0.05$). If we assume that each "composite" organic molecule contains 106 carbon atoms, based on this stoichiometry (i.e., 138:106:16:1), we calculated respiration-produced DIC (ΔDIC_{res}) using ΔAOU, ΔN, and ΔP, respectively. Each of the three ΔDIC_{res} values was then subtracted from the observed ΔDIC at each isopycnal surface, the average of the three residuals (i.e., $\Delta DIC-\Delta DIC_{res}$) was considered as C_{ant} (Table 5). Using this method, average C_{ant} accumulation across all examined isopycnals was calculated to be 8.5 ± 5.5 μmol kg^{-1} in the ~100–250 m depth interval of the water column ($C_{ant\_Redfield}$, Table 5) during the 10-year period.

Recently, Xue et al. (2015) used a multiple regression model to calculate the remineralization stoichiometry in the eutrophic northern Gulf of Mexico continental shelf. These authors obtained slightly different reaction ratios, i.e., ΔAOU:ΔDIC:ΔN:Δ*P* = 133:88:16:1. Using the approach described above and these multiple regression-generated reaction ratios, calculated C_{ant} accumulation over the 10-year period increased slightly to 11.8 ± 6.3 μmol kg^{-1} (C_{ant_Xue}, Table 5). Since overall DIC increased 29.0 ± 13.7 μmol kg^{-1} in the examined subsurface water column (Table 5), C_{ant} contributed to 30 ± 12% (Redfield) or 41 ± 10% (Xue) to the total DIC increase from the 2007 cruise to the 2017 cruise. Therefore, respiration appears to have played a more important role (59–70% of DIC increase) in acidifying the subsurface waters adjacent to the FGBNMS. As pH and Ω_{arag} are non-linear functions of DIC addition in seawater, we elected not to report individual contributions to pH and Ω_{arag} change by these two processes.

The rate of C_{ant} increase calculated using both the Redfield stoichiometry and that generated from the data-based regression model (Xue et al., 2015), i.e., 8.5–11.8 μmol kg^{-1} over the 10-year period (2007–2017), is consistent with observations in the tropical Pacific surface water (Keeling et al., 2004; Winn et al., 1998) as well as in the subtropical eastern North Atlantic (Santana-Casiano et al., 2007). As the bottom of the mixed layer can deepen seasonally (i.e., from ~20 m in summer to ~120 m in winter) due to strong wintertime wind forcing and convective mixing (Muller-Karger et al., 2015), the C_{ant} signal observed in these subsurface waters should have come from both direct Gulf seawater CO_2 uptake and horizontal transport via large scale subsurface currents that outcrop outside of this region (e.g., Rivas et al., 2005; Vidal et al., 1994).

Finally, although it is not a focus of this study, the increase in summertime AOU (i.e., decrease in dissolved oxygen concentration, Fig. 9) across the 10-year period and the elevated nutrient concentrations in 2017 compared with those in 2007 appear to imply a net loss of oxygen in these subsurface waters. Further studies are required to investigate whether this oxygen decrease was an episodic or a progressive change.

5. Conclusions

For all CCL's water samples that had three carbonate system parameters analyzed, including both the seasonal cruise samples and the 2016 rapid response cruise samples, internal consistency calculations suggest that analytical precision and accuracy were similar to those in recent, larger scale studies.

Seawater surrounding FGBNMS during the 2013–2016 study period displayed relatively narrow ranges of carbonate system parameters (pH, Ω_{arag}, and pCO_2, Fig. 3). Coral reefs within FGBNMS are bathed in well-buffered seawater with annual in-situ pH and Ω_{arag} fluctuations of < 0.15 (average 8.065 ± 0.030, $n = 99$) and < 0.8 (overall 3.698 ± 0.208, n = 99), respectively, and the latter was "adequate" for corals because of the relatively high Ω_{arag} (Guinotte et al., 2003). Despite the potential influence of nutrient-enriched, large river

discharge in this region, temperature exerted the dominant control on DIC, pCO_2, pH, and Ω_{arag} (Fig. 6), while biological activity (which included possible enhanced primary production driven by terrestrial derived nutrients) likely had a secondary effect on their variations, indicating the oligotrophic nature of this shelf environment.

Air-sea CO_2 gradients showed strong seasonality. Seawater CO_2 uptake occurred in winter and CO_2 degassing occurred in summer. If we discount the influence of episodic continental flooding, this area would be a weak CO_2 sink (-0.14 ± 1.96 mmol-C m^{-2} d^{-1}), although note the large uncertainty. Nevertheless, a change in freshwater input for a short period of time could change the mass balance as freshwater could deliver organic matter and temporarily increase surface respiration.

Based on data from three cruises that sampled subsurface waters between 2007 and 2017, we observed a greater acidification rate in the FGBNMS region than in the open oceans and the Caribbean Sea. This acidification can be attributed to both anthropogenic CO_2 uptake and elevated respiration. Using reaction stoichiometry from the literature, anthropogenic CO_2 was estimated to contribute to 30–41% of the DIC increase in the ~100–250 m depth interval of the water column while respiration accounted for the rest. In addition, it is unclear whether the observed decrease in oxygen level and buildup of respiration products were an episodic phenomenon or represented a progressive change, further studies are required to address this question.

Acknowledgements

XH was supported by a Gulf of Mexico Research Initiative grant (GOMRI-220). Data collected using this grant are publicly available through the Gulf of Mexico Research Initiative Information & Data Cooperative (GRIIDC) at https://data.gulfresearchinitiative.org (UDI: R2.x220.000:0006). Quarterly sampling that was part of the Stetson Bank long-term monitoring program was funded through Interagency Agreement E14PG00052 between the U.S. Department of the Interior (DOI), Bureau of Safety and Environmental Enforcement (BSEE) and the National Oceanic and Atmospheric Administration's National Ocean Service (NOAA-NOS), Office of National Marine Sanctuaries (ONMS), through FGBNMS, as well as the National Marine Sanctuary Foundation (NMSF). Quarterly sampling that was part of the long-term monitoring program at EFGB and WFGB was funded through Interagency Agreements M14PG00020 and M16PG00018 between U.S. DOI, Bureau of Ocean Energy Management and the NOAA-NOS, ONMS, through FGBNMS. The samples were collected under permits FGBNMS-2009-001 and FGBNMS-2014-001. NCRMP is co-funded by NOAA's Coral Reef Conservation Program (NCRMP) and Ocean Acidification Program (OAP). NCRMP sample collection and processing were conducted by T. Burton, R. Carlton, R. Clark, K. Edwards, and D. Graham. The GOMECC-1 study was supported by NOAA Global Carbon Cycle Program, and the GOMECC-3 study was supported by NOAA OAP. We thank the scientific parties on board the R/V *Ron Brown* and the R/V *Manta* for their assistance with water sample collections and field data processing, J.-Z. Zhang for sharing the GOMECC-3 nutrient data, and J. Pollack and T. Palmer for discussions on the statistical analysis. A. Mucci and two anonymous reviewers provided insightful and detailed comments on an earlier version of this manuscript, which helped to improve the quality of this manuscript significantly. The manuscript content solely reflects the opinions of the authors and do not constitute a statement of policy, decision, or position on behalf of NOAA or the US Government.

Appendix A. Supplementary data

Supplementary data to this article can be found online at https://doi.org/10.1016/j.marchem.2018.07.006.

References

Bates, N.R., 2017. Twenty years of marine carbon cycle observations at Devils Hole Bermuda provide insights into seasonal hypoxia, coral reef calcification, and ocean acidification. Front. Mar. Sci. 4, 36.
Bright, T.J., 1977. Coral reefs, nepheloid layers, gas seeps and brine flows on hard-banks in the northwestern Gulf of Mexico. In: Proc. 3rd Intl. Coral Reef Symp. pp. 39–46.
Burnham, K.P., Anderson, D.R., 2002. Model Selection and Multimodel Inference: A Practical Information-Theoretic Approach. Springer-Verlag.
Byrne, R.H., Mecking, S., Feely, R.A., Liu, X., 2010. Direct observations of basin-wide acidification of the North Pacific Ocean. Geophys. Res. Lett. 37, L02601.
Cantin, N.E., Cohen, A.L., Karnauskas, K.B., Tarrant, A.M., McCorkle, D.C., 2010. Ocean warming slows coral growth in the central Red Sea. Science 329, 322–325.
Carter, B.R., Radich, J.A., Doyle, H.L., Dickson, A.G., 2013. An automatic system for spectrophotometric seawater pH measurements. Limnol. Oceanogr.-Meth. 11, 16–27.
Clayton, T.D., Byrne, R.H., 1993. Spectrophotometric seawater pH measurements: total hydrogen ion concentration scale calibration of m-cresol purple and at-sea results. Deep-Sea Res. Pt. I 40, 2115–2129.
Coral Program, N.O.A.A., 2014. National Coral Reef Monitoring Plan. NOAA Coral Reef Conservation Program. Silver Spring, MD (39 pp).
DeBose, J.L., Nuttall, M.F., Hickerson, E.L., Schmahl, G.P., 2013. A high-latitude coral community with an uncertain future: Stetson Bank, northwestern Gulf of Mexico. Coral Reefs 32, 255–267.
Dickson, A.G., 1990. Standard potential of the reaction: AgCl(s) + $12H_2$(g) = Ag(s) + HCl(aq), and and the standard acidity constant of the ion HSO4− in synthetic sea water from 273.15 to 318.15 K. J. Chem. Thermodyn. 22, 113–127.
Dickson, A.G., Millero, F.J., 1987. A comparison of the equilibrium constants for the dissociation of carbonic acid in seawater media. Deep-Sea Res. 34, 1733–1743.
Dickson, A.G., Sabine, C.L., Christian, J.R., 2007. Guide to Best Practices for Ocean CO_2 Measurements. 3 PICES Special Publication.
Erez, J., Reynaud, S., Silverman, J., Schneider, K., Allemand, D., 2011. Coral calcification under ocean acidification and global change. In: Dubinsky, Z., Stambler, N. (Eds.), Coral Reefs: An Ecosystem in Transition. Springer, Netherlands, pp. 151–176.
Eyre, B.D., et al., 2018. Coral reefs will transition to net dissolving before end of century. Science 359, 908–911.
Gledhill, D.K., Wanninkhof, R., Millero, F.J., Eakin, M., 2008. Ocean acidification of the Greater Caribbean Region 1996–2006. J. Geophys. Res. 113, C10031.
González-Dávila, M., Santana-Casiano, J.M., González-Dávila, E.F., 2007. Interannual variability of the upper ocean carbon cycle in the Northeast Atlantic Ocean. Geophys. Res. Lett. 34, L07608.
Grasshoff, K., Kremling, K., Ehrhardt, M., 1999. Methods of Seawater Analysis. Wiley-VCH (600 pp).
Guinotte, J.M., Buddemeier, R.W., Kleypas, J.A., 2003. Future coral reef habitat marginality: temporal and spatial effects of climate change in the Pacific basin. Coral Reefs 22, 551–558.
Heuven, van, Pierrot, S.D., Rae, J.W.B., Lewis, E., Wallace, D.W.R., 2011. MATLAB Program Developed for CO_2 System Calculations. 1944–9224, ORNL/CDIAC-105b.
Hoegh-Guldberg, O., Mumby, P.J., Hooten, A.J., Steneck, R.S., Greenfield, P., Gomez, E., Harvell, C.D., Sale, P.F., Edwards, A.J., Caldeira, K., Knowlton, N., Eakin, C.M., Iglesias-Prieto, R., Muthiga, N., Bradbury, R.H., Dubi, A., Hatziolos, M.E., 2007. Coral reefs under rapid climate change and ocean acidification. Science 318, 1737–1742.
Hsu, S.A., Meindl, E.A., Gilhousen, D.B., 1994. Determining the power-law wind-profile exponent under near-neutral stability conditions at sea. J. Appl. Meteorol. 33, 757–765.
Hu, X., Beseres Pollack, J., McCutcheon, M.R., Montagna, P.A., Ouyang, Z., 2015. Long-term alkalinity decrease and acidification of estuaries in northwestern Gulf of Mexico. Environ. Sci. Technol. 49, 3401–3409.
Hu, X., et al., 2017. Effects of eutrophication and benthic respiration on water column carbonate chemistry in a traditional hypoxic zone in the Northern Gulf of Mexico. Mar. Chem. 194, 33–42.
Huang, W.J., Cai, W.J., Wang, Y., Hu, X., Chen, B., Lohrenz, S.E., Chakraborty, S., He, R., Brandes, J., Hopkinson, C.S., 2015a. The response of inorganic carbon distributions and dynamics to upwelling-favorable winds on the northern gulf of Mexico during summer. Cont. Shelf Res. 111, 211–222.
Huang, W.-J., Cai, W.-J., Wang, Y., Lohrenz, S.E., Murrell, M.C., 2015b. The carbon dioxide (CO_2) system on the Mississippi River–dominated continental shelf in the northern Gulf of Mexico – I: distribution and air-sea CO_2 flux. J. Geophys. Res.-Oceans 120, 1429–1445.
Johnston, M.A., et al., 2016. Persistence of coral assemblages at East and West Flower Garden Banks, Gulf of Mexico. Coral Reefs 35, 821–826.
Johnston, M.A., Eckert, R.J., Nuttall, M.F., Sterne, T.K., Embesi, J.A., Manzello, D.P., Hickerson, E.L., Schmahl, G.P., 2017a. Long-term monitoring at East and West Flower Garden Banks, 2013–2015. Volume 1: technical report U.S. Dept. of Interior, Bureau of Ocean Energy Management, Gulf of Mexico OCS Region, New Orleans, Louisiana OCS Study BOEM 2017–058. (186 p).
Johnston, M.A., Sterne, T.K., Eckert, R.J., Nuttall, M.F., Embesi, J.A., Walker, R., Hu, X., Hickerson, E.L., Schmahl, G.P., 2017b. Long-term monitoring at East and West Flower Garden Banks, 2016 annual report. In: Marine Sanctuaries Conservation Series ONMS-17-09. U.S. Department of Commerce, National Oceanic and Atmospheric Administration, Flower Garden Banks National Marine Sanctuary, Galveston, TX (132 pp).
Keeling, C.D., Brix, H., Gruber, N., 2004. Seasonal and long-term dynamics of the upper ocean carbon cycle at Station ALOHA near Hawaii. Global Biogeochem. Cy. 18.
Kleypas, J.A., Yates, K.K., 2009. Coral reefs and ocean acidification. Oceanography 22, 109–117.
Kleypas, J.A., Buddemeier, R.W., Gattuso, J.-P., 2001. The future of coral reefs in an age of global change. Int. J. Earth Sci. 90, 426–437.
Kutner, M., 2004. Applied Linear Regression Models. McGraw-Hill, Boston, MA.
Lang, J.C., Deslarzes, K.J.P., Schmahl, G.P., 2001. The flower garden banks: remarkable

reefs in the NW Gulf of Mexico. Coral Reefs 20, 126.
Lee, K., Choi, S.-D., Park, G.-H., Wanninkhof, R., Peng, T.-H., Key, R.M., Sabine, C.L., Feely, R.A., Bullister, J.L., Millero, F.J., Kozyr, A., 2003. An updated anthropogenic CO_2 inventory in the Atlantic Ocean. Global. Biogeochem. Cy. 17, 1116.
Liu, X., Patsavas, M.C., Byrne, R.H., 2011. Purification and characterization of meta-cresol purple for spectrophotometric seawater pH measurements. Environ. Sci. Technol. 45, 4862–4868.
Mehrbach, C., Culberson, C.H., Hawley, J.E., Pytkowicz, R.M., 1973. Measurement of the apparent dissociation constants of carbonic acid in seawater at atmospheric pressure. Limnol. Oceanogr. 18, 897–907.
Mollica, N.R., et al., 2018. Ocean acidification affects coral growth by reducing skeletal density. Proc. Natl. Acad. Sci. USA 115, 1754–1759.
Mucci, A., 1983. The solubility of calcite and aragonite in seawater at various salinities. Am. J. Sci. 283, 780–799.
Muller-Karger, F.E., et al., 2015. Natural variability of surface oceanographic conditions in the offshore Gulf of Mexico. Prog. Oceanogr. 134, 54–76.
Nuttall, M.F., Sterne, T.K., Eckert, R.J., Hu, X., Sinclair, J., Hickerson, E.L., Embesi, J.A., Johnston, M.J., Schmahl, G.P., 2017. Long-Term Monitoring at Stetson Bank, Flower Garden Banks National Marine Sanctuary, 2015 Annual Report. Marine Sanctuaries Conservation Series ONMS-17-06. U.S. Department of Commerce, National Oceanic and Atmospheric Administration, Flower Garden Banks National Marine Sanctuary, Galveston, TX (pp. 98).
Patsavas, M.C., Byrne, R.H., Liu, X., 2013. Purification of meta cresol purple and cresol red by flash chromatography: procedures for ensuring accurate spectrophotometric seawater pH measurements. Mar. Chem. 150, 19–24.
Patsavas, M.C., Byrne, R.H., Wanninkhof, R., Feely, R.A., Cai, W.-J., 2015. Internal consistency of marine carbonate system measurements and assessments of aragonite saturation state: insights from two U.S. coastal cruises. Mar. Chem. 176, 9–20.
Peng, T.-H., Wanninkhof, R., 2010. Increase in anthropogenic CO_2 in the Atlantic Ocean in the last two decades. Deep-Sea Res. Pt. I 57, 755–770.
Prytherch, J., et al., 2010. Open ocean gas transfer velocity derived from long-term direct measurements of the CO_2 flux. Geophys. Res. Lett. 37, L23607.
Rabalais, N.N., Cai, W.-J., Carstensen, J., Conley, D.J., Fry, B., Hu, X., Quiñones-Rivera, Z., Rosenberg, R., Slomp, C.P., Turner, R.E., Voss, M., Wissel, B., Zhang, J., 2014. Eutrophication-driven deoxygenation in the coastal ocean. Oceanography 27, 172–183.
Redfield, A., 1934. On the Proportions of Organic Derivatives in Sea Water and their Relation to the Composition of Plankton. James Johnstone Memorial Volume, Liverpool, pp. 176–192.
Redfield, A., 1958. The biological control of chemical factors in the environment. Am. Sci. 46, 205–222.
Rivas, D., Badan, A., Ochoa, J., 2005. The ventilation of the deep Gulf of Mexico. J. Phys. Oceanogr. 35, 1763–1781.
Robbart, M.B., Deslarzes, K., Precht, W., Aronson, R., Zimmer, B., Deis, D.R., Sinclair, J., Hickerson, E., Schmahl, G.P., Boland, G., 2008. Post-Hurricane Assessment (Hurricane Rita, September 2005) and Recovery at the East Flower Garden Bank. (Northwest Gulf of Mexico).
Sabine, C.L., Feely, R.A., Key, R.M., Bullister, J.L., Millero, F.J., Lee, K., Peng, T.-H., Tilbrook, B., Ono, T., Wong, C.S., 2002. Distribution of anthropogenic CO_2 in the Pacific Ocean. Global. Biogeochem. Cy. 16, 1083.
Santana-Casiano, J.M., González-Dávila, M., Rueda, M.-J., Llinás, O., González-Dávila, E.-F., 2007. The interannual variability of oceanic CO_2 parameters in the Northeast Atlantic subtropical gyre at the ESTOC site. Global. Biogeochem. Cy. 21, GB1015.
Takahashi, T., Sutherland, S.C., Sweeney, C., Poisson, A., Metzl, N., Tilbrook, B., Bates, N., Wanninkhof, R., Feely, R.A., Sabine, C., Olafsson, J., Nojiri, Y., 2002. Global sea–air CO2 flux based on climatological surface ocean pCO2, and seasonal biological and temperature effects. Deep-Sea Res. Pt. II 49, 1601–1622.
Takahashi, T., et al., 2009. Climatological mean and decadal change in surface ocean pCO_2, and net sea-air CO_2 flux over the global oceans. Deep-Sea Res. II 56, 554–577.
Uppström, L.R., 1974. The boron/chlorinity ratio of deep-sea water from the Pacific Ocean. Deep-Sea Res. Oceanogr. Abstr. 21, 161–162.
Vidal, V.M.V., Vidal, F.V., Hernadez, A.F., Meza, E., Zambrano, L., 1994. Winter water mass distributions in the Western Gulf of Mexico affected by a colliding anticyclonic ring. J. Oceanogr. 50, 559–588.
Wang, Z.A., Wanninkhof, R., Cai, W.-J., Byrne, R.H., Hu, X., Peng, T.-H., Huang, W.-J., 2013. The marine inorganic carbon system along the Gulf of Mexico and Atlantic coasts of the United States: insights from a transregional coastal carbon study. Limnol. Oceanogr. 58, 325–342.
Wanninkhof, R., 1992. Relationship between wind speed and gas exchange over the ocean. J. Geophys. Res. 97, 7373–7382.
Wanninkhof, R., 2014. Relationship between wind speed and gas exchange over the ocean revisited. Limnol. Oceanogr.-Meth. 12, 351–362.
Wanninkhof, R., McGillis, W.R., 1999. A cubic relationship between air-sea CO_2 exchange and wind speed. Geophys. Res. Lett. 26, 1889–1892.
Wanninkhof, R., Asher, W.E., Ho, D.T., Sweeney, C., McGillis, W.R., 2009. Advances in quantifying air-sea gas exchange and environmental forcing. Annu. Rev. Mar. Sci. 1, 213–244.
Wanninkhof, R., Doney, S.C., Bullister, J.L., Levine, N.M., Warner, M., Gruber, N., 2010. Detecting anthropogenic CO_2 changes in the interior Atlantic Ocean between 1989 and 2005. J. Geophys. Res. 115, C11028.
Wanninkhof, R., et al., 2015. Ocean acidification along the Gulf Coast and East Coast of the USA. Cont. Shelf Res. 98, 54–71.
Weiss, R.F., 1970. The solubility of nitrogen, oxygen and argon in water and seawater. Deep-Sea Res.: Oceanogr. Abstr. 17, 721–735.
Weiss, R.F., 1974. Carbon dioxide in water and seawater: the solubility of a non-ideal gas. Mar. Chem. 2, 203–215.
Winn, C.D., Li, Y.-H., Mackenzie, F.T., Karl, D.M., 1998. Rising surface ocean dissolved inorganic carbon at the Hawaii Ocean time-series site. Mar. Chem. 60, 33–47.
Woosley, R.J., Millero, F.J., Wanninkhof, R., 2016. Rapid anthropogenic changes in CO_2 and pH in the Atlantic Ocean: 2003–2014. Global. Biogeochem. Cy. 30, 70–90.
Xue, J., Cai, W.-J., Hu, X., Huang, W.-J., Lohrenz, S.E., Gundersen, K., 2015. Temporal variation and stoichiometric ratios of organic matter remineralization in bottom waters of the northern Gulf of Mexico during late spring and summer. J. Geophys. Res.-Oceans 120, 8304–8326.
Zhang, J.-Z., Kelble, C.R., Fischer, C.J., Moore, L., 2009. Hurricane Katrina induced nutrient runoff from an agricultural area to coastal waters in Biscayne Bay, Florida. Estuar. Coast. Shelf S. 84, 209–218.